

Evaluation of a measure on the quasi-steady state assumption of Collisional Radiative Models via Intrinsic Low Dimensional Manifold Technique

Efe Kemaneci, Emile Carbone, Wouter Graef, Jan van Dijk, Gerrit M W Kroesen
Department of Applied Physics, Eindhoven University of Technology, The Netherlands
 (Dated: December 1, 2015)

Collisional and radiative dynamics of a plasma is exposed by so-called Collisional Radiative Models [1] that simplify the chemical kinetics by quasi-steady state assignment on certain types of particles. The assignment is conventionally based on the classification of the plasma species by the ratio of the transport to the local destruction frequencies. We show that the classification is not exact due to the role of the time-dependent local production, and a measure is necessary to confirm the validity of the assignment. The main goal of this study is to evaluate a measure on the quasi-steady state assumptions of these models. Inspired by a chemical reduction technique called Intrinsic Low Dimensional Manifolds [2, 3], an estimate local source is provided at the transport time-scale. This source is a deviation from the quasi-steady state for the particle and its value is assigned as an error of the quasi-steady state assumption. The propagation of this error on the derived quantities is formulated in the Collisional Radiative Models. Based on the error a novel technique is proposed to discriminate the quasi-steady states. The developed analysis is applied to mercury and argon fluorescent lamps separately and the corresponding errors are presented. We observe that the novel and conventional technique agrees for most of the excited levels but disagrees for a few low energy excited states.

I. INTRODUCTION

Plasmas are extensively employed for the purpose of surface treatment [4, 5] and lighting applications [6]. Their collective feature is a large number of locally interacting species such as excited atomic or molecular states and chemical reactants. This characteristic induces numerical difficulties such as heavy computational load and stiffness; therefore, long-lasting simulations and troublesome convergences appear. Although models that contain large number of species are still viable, these difficulties persuade reduction of this number.

A naive approach in reducing the number of species is to ignore low-valued particle densities. Although it decreases the computational load and relieve the stiffness, it may lock essential reaction channels in the physical system. Hence, reduction techniques respecting all the local interactions are obligatory. *Collisional Radiative Model* (CRM) is such a reduction method, which is widely used in low-temperature atomic plasmas. It focuses on the interplay between collisional and radiative processes. The technique was commenced by Bates *et al.* [7] and improved further by various authors [8–10]. So-called *Local Chemistry* (LC) species already equilibrated to *Quasi-Steady State* (QSS) in local chemistry at the transport time-scale and it uses this fact to determine a reduced set of species and effective reaction rates.

Reduction methods are utilised not only in the area of plasma science but also in other fields with overlapping peculiarity [3, 11, 12]. Though developed independently, some of these techniques are remarkably similar. For example, in mathematical biology, some [11] use QSS assumptions, while certain combustion models [13] similarly assume partial equilibrium and steady state. Another reduction method that is extensively employed in combustion engine flame models is *Intrinsic Low Dimen-*

sional Manifold (ILDM) technique. It was initiated by Maas *et al.* [3] and studied further by numerous authors [2, 14]. It makes use of characteristic principal frequencies of local interactions to determine an asymptotic state of the mass fractions that leads the chemical reduction.

CRMs are strong tools with a low computational load for the investigation of the plasma species and their interactions, however, they suffer from a couple of inadequacies. The first one is the LC condition, which discriminates the species quickly reaching QSS. It is based on the ratio of the transport to local destruction frequencies. Since it excludes the role of the time-dependent local production, it is insufficient in the assignments. The second inadequacy is the deviations from the QSS assumption that perturbs the derived quantities in the CRM. These deviations and the resulting perturbations are ignored in the conventional CRM formalism. In this study, these inadequacies are addressed with the aid of the ILDM technique.

Inspired by the ILDM technique, we estimate a local source at the transport time-scale and assign it as an error on the QSS assumption of CRMs. This error quantifies a deviation from the assumption and its influence on the derived quantities of CRM is formulated. Furthermore, we propose a novel LC condition based on the error with a consistent measure that incorporates the local production. We apply this new approach to Ar- or Hg-containing fluorescent lamps separately. The comparison of the conventional and new LC conditions is presented together with the error. In section II governing equations are analysed for the plasma under investigation and the main points characterising the LC particles are discussed. Section III introduces CRM and section IV shows the analysis in a diagonal basis, which is similar to the first step of the ILDM technique. In section V we define the error and introduce the novel LC condition. Section VI describes the Ar and Hg plasma parameters and section

VII presents the results. In section VIII summary and conclusion are given.

II. PARTICLE BALANCES

The densities of the species are governed by particle balance equations. For species i , it is given by

$$\frac{\partial n_i}{\partial t} + \vec{\nabla} \cdot \vec{\Gamma}_i = S_i, \quad (1)$$

where n_i is particle density of species, $\vec{\Gamma}_i$ its particle flux and S_i its net production rate. The first term expresses the time evolution of densities while the second one represents convective, diffusive transport. The right-hand side corresponds to the chemical reactions. This term explicitly couples several species to each other. Additionally, the transport term may couple them in the case of multicomponent diffusion [15], which is not considered here.

We introduce the notation used in [8] in order to compare the various chemical processes. Since losses are proportional to n_i , the source can be written in terms of the destruction and the production

$$S_i = \mathcal{P}_i - \mathcal{D}_i n_i, \quad (2)$$

where \mathcal{D}_i represents the destruction frequency and \mathcal{P}_i is the production rate. In general, these are functions of all other densities and various system parameters. In equilibrium, the source satisfies

$$S_i = 0 \quad (3)$$

and leads the equilibrium density

$$n_i^{Eqb} = \mathcal{P}_i / \mathcal{D}_i. \quad (4)$$

Furthermore, the transport frequency of species i is defined as

$$\nu_{tr,i} = \frac{\vec{\nabla} \cdot \vec{\Gamma}_i}{n_i}. \quad (5)$$

As a result, the particle balances can be written as

$$\frac{\partial n_i}{\partial t} + \nu_{tr,i} n_i = \mathcal{P}_i - \mathcal{D}_i n_i. \quad (6)$$

The ratio of transport to destruction frequencies determines dominant process among them. Keeping this in

mind, we introduce Damköhler number $D_{a,i} = \frac{\mathcal{D}_i}{\nu_{tr,i}}$, then equation (6) further takes the form

$$\frac{1}{\mathcal{D}_i} \frac{\partial n_i}{\partial t} + \frac{n_i}{D_{a,i}} = n_i^{Eqb} - n_i. \quad (7)$$

For large Damköhler number, $D_{a,i} \gg 1$ the transport term can be ignored in equation (6):

$$\frac{1}{\mathcal{D}_i} \frac{\partial n_i}{\partial t} = \frac{\mathcal{P}_i}{\mathcal{D}_i} - n_i. \quad (8)$$

If \mathcal{P}_i is constant of time, then n_i^{Eqb} is reached exponentially in characteristic time $1/\mathcal{D}_i$, which is long before the transport time-scale $\tau_{tr} = 1/\nu_{tr,i}$. Bates *et al.* [7] realised that these species, called *Local Chemistry* (LC) species in CRM, are initially dominated by the local source. In this case, the destruction diminishes the net production rate and they reach *Quasi-Steady State* (QSS)

$$S_i = 0. \quad (9)$$

In order to manipulate the coupled particle balance equations more conveniently, vector notation is introduced. Let $\mathbf{n} = \{n_i\}$ be the column vector of species densities n_i . Similarly, the transport and source terms are $\vec{\nabla} \cdot \vec{\Gamma} = \{\vec{\nabla} \cdot \vec{\Gamma}_i\}$, $\mathbf{S} = \{S_i\}$. With this notation, the particle balance equations can be written as

$$\frac{\partial \mathbf{n}}{\partial t} + \vec{\nabla} \cdot \vec{\Gamma} = \mathbf{S}. \quad (10)$$

This work focuses on atomic *Electron Excitation Kinetics* (EEK) plasmas that are defined by van der Mullen [8]. The chemical reactions in these plasmas are dominated by radiative and electron induced transitions between atomic levels. Besides the ground state, the ion and the electron; the excited levels play a role in such reactions. Explicit forms of these reactions are listed in table (I). One common assumption in EEK plasmas is that the electrons act as “external agents” with density n_e and temperature T_e [8]. They are not included in density vector \mathbf{n} .

Since the source terms of the other species are linear in their densities, these can be written as

$$\mathbf{S} = \mathbf{M}(n_e, T_e) \mathbf{n}. \quad (11)$$

The source matrix \mathbf{M} is composed of the reaction frequencies, combining equation (11) with table I yields

Label	Reaction	Rate	Name
R1	$A(i) + e \rightarrow A(j) + e, (i < j)$	$n_i n_e k_{ij}$	Electron impact excitation
R2	$A(i) + e \rightarrow A(j) + e, (i > j)$	$n_i n_e k_{ij}$	Electron impact de-excitation
R3	$A(i) + e \rightarrow A^+ + 2e$	$n_i n_e k_{i'+}$	Electron impact ionisation
R4	$A^+ + 2e \rightarrow A(j) + e$	$n_{'+} n_e^2 K_{'+i}^{(3)}$	Three particle recombination
R5	$A(i) \rightarrow A(j) + h\nu$	$n_i A_{ij}^*$	Spontaneous emission
R6	$A(i) + h\nu \rightarrow A(j) + 2h\nu$	$n_i \beta_{ij}(\nu)$	Stimulated emission
R7	$A(j) + h\nu \rightarrow A^+ + e$	$n_j \alpha_j$	Photoionisation
R8	$A^+ + e \rightarrow A(j) + h\nu$	$n_{'+} n_e \alpha_j$	Radiative recombination

TABLE I. Chemical reactions in atomic pure EEK plasmas. A and e represents atom and electrons, while i specify the neutral species and $+$ ions. These neutral species are composed of ground and excited levels of the atom. In this work, we neglect the photoionisation and stimulated emission.

$$M_{ij} = \begin{cases} -\left[\sum_{p \neq j} n_e k_{jp} + n_e k_{j'+} \sum_{p \leq j} A_{jp}^*\right] & i = j & \text{R1, R2, R3, R5} \\ n_e k_{ji} + A_{ji}^* & i < j & \text{R1, R5} \\ n_e k_{ji} & i > j & \text{R2} \\ n_e k_{ji} & i = ' + ' & \text{R3} \\ n_e^2 K_{ji}^{(3)} + n_e \alpha_i & j = ' + ' & \text{R4, R8} \end{cases} \quad (12)$$

where photoionisation and stimulated emission are not included. For $i \neq j$, M_{ij} is the production frequency of state i from j and M_{ii} is the destruction frequency of state i . With this notation, the production term in equation (2) is $\mathcal{P}_i = \sum_{j \neq i} M_{ij} n_j$ while the destruction frequency is $\mathcal{D}_i = M_{ii}$

III. COLLISIONAL RADIATIVE MODELS

Solving too many coupled particle balance equations causes heavy computational load and stiffness. In order to prevent this, CRMs reduce the number of species, for which these equations are solved without neglecting the species or their role in the reactions. The model relies upon a classification of species into two types: *Local Chemistry* (LC) and *Transport Sensitive* (TS). LC species satisfies $D_{a,i} \gg 1$ and reaches QSS (equation (9)) before the transport time-scale. They feature vanishing local sources while the others do not.

The relations between LC and TS species is re-formulated by van Dijk *et al.* [10] in the following analysis. Reordering the species indices such that the TS species are at the top of the vector, \mathbf{S} and \mathbf{n} can be decomposed as [10]:

$$\mathbf{S} = \begin{bmatrix} \mathbf{S}_t \\ \mathbf{S}_l \end{bmatrix}, \quad \mathbf{n} = \begin{bmatrix} \mathbf{n}_t \\ \mathbf{n}_l \end{bmatrix}, \quad (13)$$

where l labels the LC and t labels the TS species. Imposing QSS assumption on the LC species $\mathbf{S}_l = \mathbf{0}$ and similarly decomposing the source matrix \mathbf{M} , equation (11)

becomes

$$\begin{bmatrix} \mathbf{S}_t \\ \mathbf{0} \end{bmatrix} = \begin{bmatrix} \mathbf{M}_{tt} & \mathbf{M}_{lt} \\ \mathbf{M}_{tl} & \mathbf{M}_{ll} \end{bmatrix} \begin{bmatrix} \mathbf{n}_t \\ \mathbf{n}_l \end{bmatrix}. \quad (14)$$

This yields two sets of equations;

$$\mathbf{S}_t = \mathbf{M}_{tt} \mathbf{n}_t + \mathbf{M}_{lt} \mathbf{n}_l, \quad (15)$$

$$\mathbf{0} = \mathbf{M}_{tl} \mathbf{n}_t + \mathbf{M}_{ll} \mathbf{n}_l. \quad (16)$$

Inverting equation (16) shows that the LC densities depend linearly on the TS densities

$$\mathbf{n}_l = -(\mathbf{M}_{ll}^{-1} \mathbf{M}_{tl}) \mathbf{n}_t. \quad (17)$$

Hence, once the TS densities are known, the complete state of the plasma is available with this linear relation. Moreover, putting this relation in equation (15) we introduce an effective TS source term

$$\mathbf{S}_t = (\mathbf{M}_{tt} - \mathbf{M}_{lt} \mathbf{M}_{ll}^{-1} \mathbf{M}_{tl}) \mathbf{n}_t. \quad (18)$$

The first term on the right-hand side represents the direct processes between the TS states, while the second term describes *ladder-like* transitions, that is via the LC states. Equations (17) and (18) allow to take the LC states into account without solving their balance equations.

In spite of their wide usage CRMs contain two weak points. Firstly, the classification condition of LC species ($D_{a,l} \gg 1$) is not always sufficient: Since the local production, \mathcal{P}_l , is a function of all other densities (see equations (8, 9)), it is not constant in time. As a consequence, the exponential decay to the equilibrium density with characteristic time-scale $1/\mathcal{D}_l$ is not valid. Secondly, the

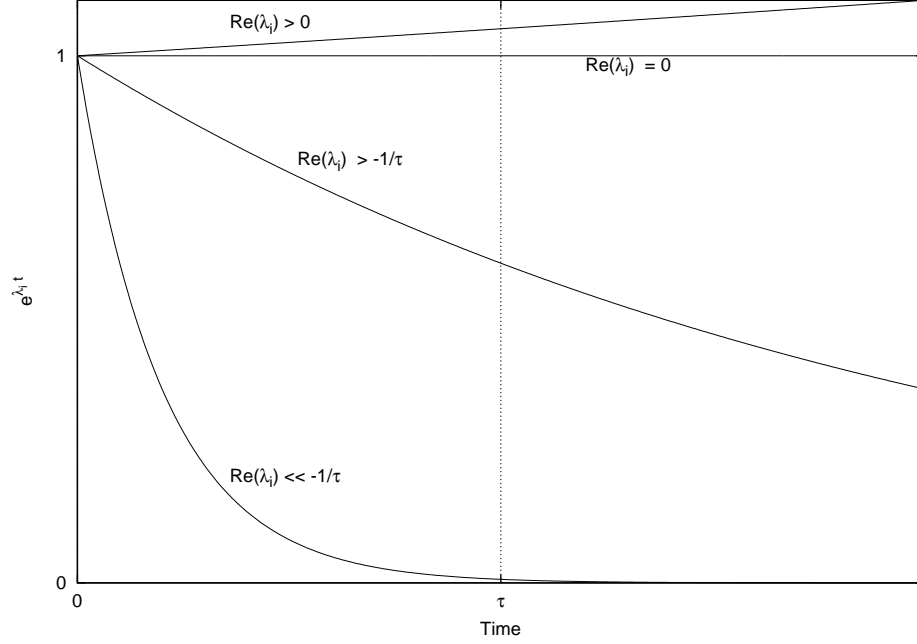


FIG. 1. The behaviour of pseudo-density \bar{n} for distinct real eigenvalues. The positive eigenvalues cause exponential growth while the negative ones induce exponential decay. Comparison with the external time-scale τ reveals pace of the decay.

deviations from the assumption $\mathbf{S}_l = \mathbf{0}$ are not quantified. These deviations may be significant and lead perturbations in the LC densities through equation (17) that propagate into the TS sources via equation (18). In following sections, we estimate these deviations thus define an error for the QSS assumption. We also quantify the resultant perturbations on equations (17, 18) and propose a novel condition to classify the LC species. Rudimentary aspects of the estimation and the assignment are developed in section IV while the error and the novel LC condition are defined in section V.

IV. DIAGONAL BASIS

Similar to the plasma sciences, the combustion engineering studies physical systems containing a large number of species that interact with complex chemical kinetics. Aforementioned numerical difficulties also arise in the models and Maas *et al.* [3] introduces ILDM technique to reduce the number of species. Adapting the notions of the ILDM technique, we introduce a diagonal basis to analyse the particle balances. Settling in this basis, decoupled set of equations are acquired with a characteristic time-scale assigned to each. This fact allows a classification of those equilibrated at a time-scale and forms the backbone of the error definition.

The technique starts with an analysis of source matrix. In order to investigate the chemical nature of the particle balances, the transport term is omitted in equation (10)

for the time being [3]:

$$\frac{\partial \mathbf{n}}{\partial t} = \mathbf{M} \mathbf{n}. \quad (19)$$

Assuming that the matrix \mathbf{M} is diagonalisable, we have

$$\mathbf{M}(n_e, T_e) = \mathbf{V} \mathbf{\Lambda} \mathbf{V}^{-1} \quad (20)$$

where \mathbf{V} is a non-singular matrix, whose columns are the eigenvectors, and $\mathbf{\Lambda} = \text{diag}[\lambda_i]$ is a diagonal matrix that contains the corresponding eigenvalues. These matrices are functions of n_e and T_e like \mathbf{M} , although we leave out the parameters for readability.

Substitution of equation (20) into equation (19) and left multiplication with \mathbf{V}^{-1} yields

$$\mathbf{V}^{-1} \frac{\partial \mathbf{n}}{\partial t} = \mathbf{\Lambda} \mathbf{V}^{-1} \mathbf{n}. \quad (21)$$

Furthermore, let τ_M be the \mathbf{M} matrix time-scale, which represents how quick it changes, and scales with how fast electron density and temperature alters. For time-scales $t \ll \tau_M$, the variations of the source matrix are negligible. As a result, its eigenvalues and eigenvectors do not vary significantly in time. This leads to the form

$$\frac{\partial (\mathbf{V}^{-1} \mathbf{n})}{\partial t} = \mathbf{\Lambda} (\mathbf{V}^{-1} \mathbf{n}). \quad (22)$$

This suggests the introduction of alternative density variables $\bar{\mathbf{n}}$ according to

$$\bar{\mathbf{n}} = \mathbf{V}^{-1} \mathbf{n}, \quad (23)$$

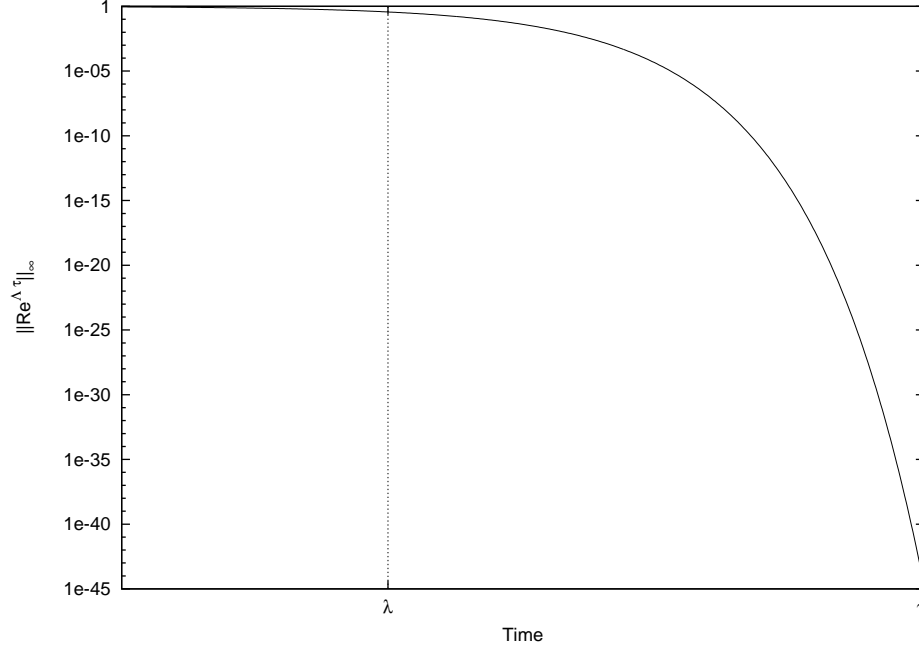


FIG. 2. The upper limit for the infinite norm of the fast pseudo-density, $\|\bar{\mathbf{n}}_f\|_\infty / n \leq \|\mathbf{R}e^{\Lambda\tau}\|_\infty$, through time. For the external time-scale satisfying $|1/\lambda| = 0.01\tau$, $\mathbf{n}_f(\tau)$ is negligible.

which we call pseudo-densities. Substitution into equation (22) yields

$$\frac{\partial \bar{\mathbf{n}}}{\partial t} = \mathbf{\Lambda} \bar{\mathbf{n}}. \quad (24)$$

Since $\mathbf{\Lambda}$ is diagonal, the equations for $\bar{\mathbf{n}}$ are decoupled and their treatment is relatively easy compared to those in original basis. For times $t \ll \tau_M$, the eigenvalues are constant and integration of equation (24) yields

$$\bar{\mathbf{n}}(t) = e^{\mathbf{\Lambda}t} \bar{\mathbf{n}}(0). \quad (25)$$

In other words, each pseudo-species labelled by i satisfies

$$\bar{n}_i(t) = e^{\lambda_i t} \bar{n}_i(0), \quad (26)$$

where we used the component notation for the sake of simplicity.

A. Classification of pseudo-densities

The particular behaviour of each pseudo-density \bar{n}_i is determined by the corresponding eigenvalue λ_i , the inverse of which represents characteristic time-scale of the equation. Obviously, a zero eigenvalue yields time invariant behaviour $\bar{n}_i(t) = \bar{n}_i(0)$, while a negative real part of the eigenvalue imposes exponential decay and estimates a decay frequency, $Re|\lambda_i|$ (see Figure 1). Comparing the corresponding decay time-scale to previously determined time parameter τ , the pseudo-densities with smaller time-scales have already equilibrated to their asymptotic value: 0.

Following these observations, we classify three type of pseudo-densities for a given time parameter τ , for instance, the transport time-scale. (1) Fast pseudo-densities possess eigenvalues with $Re(\lambda_i) \ll -1/\tau$ and they vanish at the time parameter: $\bar{n}_i(\tau) \approx 0$. The approximation asymptotically turns into equality. (2) Invariant pseudo-densities have a zero eigenvalue, and they are constants in time. (3) Otherwise, they are termed as slow pseudo-densities and these are still dynamically active.

Eigenvalue	Type	Behaviour
$Re(\lambda_i) \ll -1/\tau$	Fast	$\bar{n}_i(\tau) \approx 0$
$\lambda_i = 0$	Invariant	$\frac{d\bar{n}_i}{dt} = 0$
Else	Slow	Not known.

(27)

The pseudo-densities are linear combinations of the real densities and follow certain characteristics of the source matrix. The time invariant pseudo-densities represent the conservation of the total number of the particles in the (sub-) set of reactions. Decaying pseudo-densities represent the equilibrium of chemical processes. The imaginary part of the eigenvalue means oscillatory pseudo-density while the positive real part induces exponential growth. The oscillatory and growing pseudo-densities are not observed for the analysed systems, hence they are not treated. Since most of the physical systems eventually equilibrate, the absence of these eigenvalues is expected.

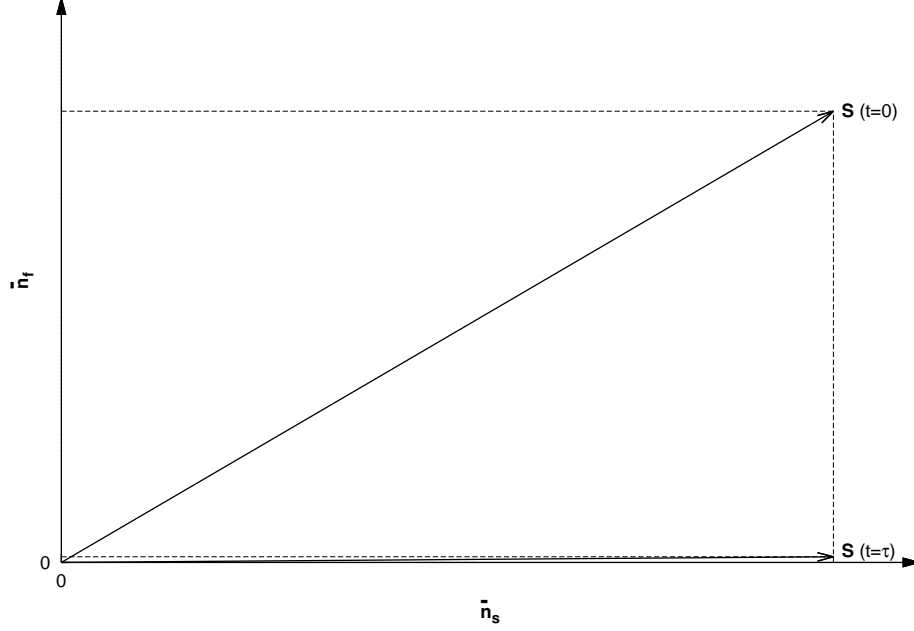


FIG. 3. A depiction of the source \mathbf{S} in the density space that is spanned by pseudo-densities. The fast component vanishes at time-scale τ .

B. Reconfiguration in the density space

In this section, we reconfigure the density space based on the classification of the pseudo-densities at the time-scale τ . Firstly, we introduce a diagonal reduction matrix $\mathbf{R}(\tau)$

$$R_{ii} = \begin{cases} 1 & \text{if } i \in \{ \text{"Fast"} \} \\ 0 & \text{else.} \end{cases} \quad (28)$$

This matrix defines fast $\bar{\mathbf{n}}_f(\tau)$ and slow $\bar{\mathbf{n}}_s(\tau)$ components of the pseudo-density $\bar{\mathbf{n}}(\tau)$:

$$\bar{\mathbf{n}}_f(\tau) = \mathbf{R}(\tau)e^{\Lambda\tau}\bar{\mathbf{n}}(0), \quad (29)$$

$$\bar{\mathbf{n}}_s(\tau) = (\mathbf{I} - \mathbf{R}(\tau))e^{\Lambda\tau}\bar{\mathbf{n}}(0), \quad (30)$$

where \mathbf{I} is the identity matrix and $\bar{\mathbf{n}}$ satisfies

$$\bar{\mathbf{n}}(\tau) = \bar{\mathbf{n}}_s(\tau) + \bar{\mathbf{n}}_f(\tau). \quad (31)$$

The fast component $\bar{\mathbf{n}}_f(\tau)$ contains all fast pseudo-densities and zero otherwise, while $\bar{\mathbf{n}}_s(\tau)$ includes the rest. Furthermore, they associate with the original density by the relations

$$\bar{\mathbf{n}}_f(\tau) = \mathbf{R}(\tau)\mathbf{V}^{-1}\mathbf{n}(\tau), \quad (32)$$

$$\bar{\mathbf{n}}_s(\tau) = (\mathbf{I} - \mathbf{R}(\tau))\mathbf{V}^{-1}\mathbf{n}(\tau). \quad (33)$$

This form partitions any density-dependent quantity into the fast and the slow components. Accordingly, using the relation (11), the source at τ is given by

$$\mathbf{S}(\tau) = \mathbf{M}\mathbf{V}\bar{\mathbf{n}}_s(\tau) + \mathbf{M}\mathbf{V}\bar{\mathbf{n}}_f(\tau). \quad (34)$$

This configuration is based on the two different regions of the density space, and each one is described by one type of the pseudo-density. (1) The fast region is emptied before τ and, for any density-dependent quantity, its corresponding component is depleted. (2) The slow one, however, is dominantly occupied around the time-scale τ .

The fast pseudo-densities are classified by their vanishing value at τ (see Figure 2) and imposing this, the pseudo-density $\bar{\mathbf{n}}(\tau)$ is approximately described by the slow component

$$\bar{\mathbf{n}}(\tau) \approx \bar{\mathbf{n}}_s(\tau). \quad (35)$$

Similarly, implementing this in the source components leads to the approximation (depicted in Figure 3)

$$\mathbf{S}(\tau) \approx \mathbf{M}\mathbf{V}\bar{\mathbf{n}}_s(\tau). \quad (36)$$

Furthermore, we express the source in terms of the original density, by defining a slow matrix, $\mathbf{M}^s(\tau) = \mathbf{M}\mathbf{V}(\mathbf{I} - \mathbf{R})\mathbf{V}^{-1}$,

$$\mathbf{S}(\tau) \approx \mathbf{M}^s\mathbf{n}(\tau). \quad (37)$$

C. Role of the transport

In the previous analysis, we omitted the transport in the particle balances and focused on the local source. In this section, we introduce an effective transport term and analyse its effect on the pseudo-densities. Firstly, we assign a hypothetical transport frequency to all species

$$\vec{\nabla} \cdot \vec{\Gamma} = \nu_{tr}\mathbf{n}, \quad (38)$$

and the particle balances take the form

$$\frac{\partial \mathbf{n}}{\partial t} = \mathbf{M}\mathbf{n} - \nu_{tr}\mathbf{n}. \quad (39)$$

By diagonalisation of \mathbf{M} we acquire equation (26) in a new form

$$\bar{n}_i(\tau) = e^{(\tau\lambda_i - \tau\nu_{tr})}\bar{n}_i(0), \quad (40)$$

which defines the role of the effective transport on the pseudo-densities.

Since the fast pseudo-species are defined by the relation $\tau|Re(\lambda_i)| \gg 1$, the transport frequency that satisfies $\tau\nu_{tr} \leq 1$ does not affect their behaviour. If it fulfils $\tau\nu_{tr} \gg 1$, the transport is relatively quick and the fast pseudo-density vanished long before time τ . Otherwise, the transport does not play a role. Furthermore, such a transport imposes that the invariant pseudo-density is no longer constant in time but exponentially decreases. In the case that $\tau\nu_{tr} \gg 1$, it is classified as a fast pseudo-density and otherwise it is a slow pseudo-density. A transport frequency such that $\tau\nu_{tr} > 1$ switches the slow pseudo-densities to fast if it also satisfies $\tau \gg 1/(|Re(\lambda_i)| + \nu_{tr})$. On the other hand, the slow behaviour does not change for $\tau\nu_{tr} \leq 1$, unless it is very close to being classified as fast.

In conclusion, the transport does not change the behaviour and classification of the pseudo-densities for $\tau/\nu_{tr} \leq 1$. Otherwise, it may shift the fast behaviour earlier in time and should also be taken into account. This implies that the source approximation is still valid at $\tau = \tau_{tr}$, independent of the transport

$$\mathbf{S}(\tau_{tr}) \approx (\mathbf{M}^s\mathbf{n})(\tau_{tr}). \quad (41)$$

As a result, we have an approximate density-dependent source that is defined at the transport time-scale τ_{tr} .

Note that the transport frequency certainly differs for ions due to the ambipolar electric field. Since the ion transport frequency is larger compared to that of neutrals [16], $\tau/\tau_{tr,ion} < 1$ is already satisfied if $\tau/\tau_{tr} \leq 1$.

V. QSS ERROR OF LC LEVELS

CRMs assume that the LC levels have already reached QSS at τ_{tr} , due to their large Damköhler number:

$$\mathbf{S}_l|_{\tau_{tr}} = \mathbf{0}, \quad (42)$$

which is based on a production term that is constant in time (see equations (8, 9)). Furthermore, the analysis in the diagonal basis assigns an approximate, density-dependent nonzero value to the source

$$\mathbf{S}_l|_{\tau_{tr}} \approx (\mathbf{M}^s\mathbf{n})_l(\tau_{tr}). \quad (43)$$

Regarding this, we use the latter to quantify the deviation from the assumption and define its absolute as the

error that is made by the QSS assumption of the LC levels. Consistent QSS error at the transport time-scale is given by the relation

$$(\mathbf{e}_Q)_l(\tau_{tr}) = |(\mathbf{M}^s\mathbf{n})_l|, \quad (44)$$

where $|\cdot|$ represents the absolute value.

Furthermore, replacing it with zero sources in equation (15), the error also propagates through the following CRM relations. The mapping between TS and LC (equation (17)) perturbs with

$$\delta\mathbf{n}_l(\tau_{tr}) = \mathbf{M}_{ll}^{-1}(\mathbf{e}_Q)_l \quad (45)$$

while the effective TS source - equation (18) - perturbs with

$$\delta\mathbf{S}_t(\tau_{tr}) = \mathbf{M}_{lt}\mathbf{M}_{ll}^{-1}(\mathbf{e}_Q)_l. \quad (46)$$

A. Density-independent QSS error and novel LC condition

Let \mathbf{M}_i^s be the i_{th} row of \mathbf{M}^s . The QSS error, $(\mathbf{e}_Q)_i$, is the inner product of \mathbf{M}_i^s and \mathbf{n} and it satisfies the Hölder's inequality

$$(\mathbf{e}_Q)_i(\tau_{tr}) \leq \|\mathbf{M}_i^s\|_1 \|\mathbf{n}\|_1, \quad (47)$$

where $\|\cdot\|_1$ represents the 1-norm of a vector. Since the 1-norm of the density vector is the total density, n , this reduces to the form

$$(\mathbf{e}_Q)_i(\tau_{tr}) \leq (\mathbf{e}_Q^1)_i(\tau_{tr})n, \quad (48)$$

where we define density-independent consistent QSS error of LC species i

$$(\mathbf{e}_Q^1)_i(\tau_{tr}) = \|\mathbf{M}_i^s(\tau_{tr})\|_1. \quad (49)$$

Together with n , it determines the upper bound for the density-dependent error and in case the density values are not available, it can be used instead.

Furthermore, we define a novel LC condition based on the density-independent consistent QSS error. In order to overcome the arbitrary scale of the error, which is intrinsically determined by each system, a dimensionless QSS error is defined by the relation

$$\widehat{(\mathbf{e}_Q)}_i(\tau_{tr}) = \frac{(\mathbf{e}_Q)_i(\tau_{tr})}{n\zeta}, \quad (50)$$

where ζ is a non-dimensionalisation constant with unit 1/s. The inequality (48) suggests that

$$\widehat{(\mathbf{e}_Q)}_i(\tau_{tr}) \leq e_i(\tau_{tr}), \quad (51)$$

where we define a dimensionless error number

$$e_i(\tau_{tr}) = \frac{(\mathbf{e}_Q^1)_i(\tau_{tr})}{\zeta}. \quad (52)$$

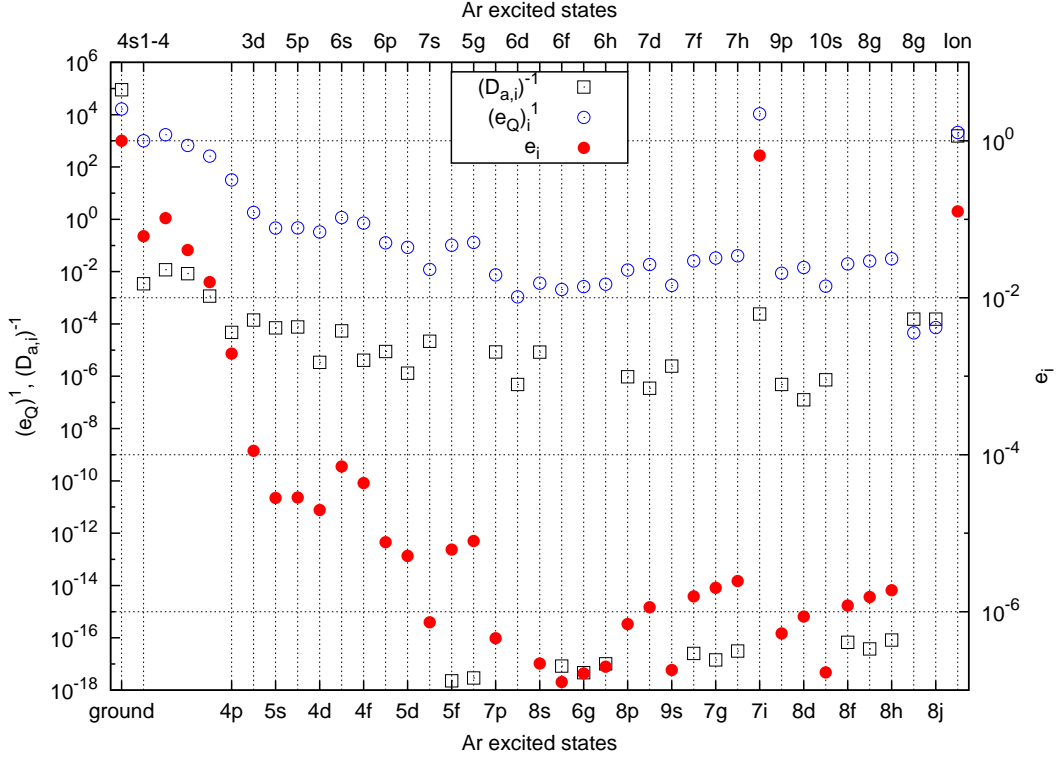


FIG. 4. (Argon plasma) The density-independent consistent QSS error $(\mathbf{e}_Q)_i^1$, the inverse of Damköhler number $(D_{a,i})^{-1}$ and the error number e_i for numbered species (i). Note the double y-axes with different scales. The transport time-scale is $\tau_{tr} = 5.20 \times 10^{-04}$ s calculated from equation (53).

Parameters	Ar	Hg
σ	10^{-19} m^2	10^{-19} m^2
n	10^{22} m^{-3}	10^{22} m^{-3}
R	$2.0 \times 10^{-2} \text{ m}$	$2.0 \times 10^{-2} \text{ m}$
L	1.80 m	1.80 m
T_e	1 eV	1 eV
T_h	300 K	300 K
τ_{tr}	$5.20 \times 10^{-04} \text{ s}$	$1.17 \times 10^{-03} \text{ s}$
n_e	$1.0 \times 10^{18} \text{ m}^{-3}$	$1.0 \times 10^{18} \text{ m}^{-3}$

TABLE II. Main EEK atomic plasma parameters.

If this number is sufficiently small compared to unity, it ensures a negligible dimensionless QSS error relative to ζ . In this respect, we classify LC level as a species that satisfy

If $e_i \ll 1$ then i is an LC level.

For the ζ , we use the density-independent error of the ground state, $(\mathbf{e}_Q^1)_0$, with the assumption that the ground state is a TS level with the highest density-independent error. Since the ions do have complex transport phenomena, such as ambipolar diffusion, we do not classify them but assume that they are TS.

VI. MODEL SETUP

The QSS errors and the error numbers are investigated in the cylindrical column of a fluorescent lamp. The plasma is contained in the radius $R = 2.0 \times 10^{-2}$ m within the length $L = 1.80$ m. We analyse either argon or mercury based atomic discharges, neglecting spatial inhomogeneities and the sheath phenomena. Additionally, we assume the two-temperature plasma condition of the Maxwellian distribution functions, together with the electron temperature $T_e = 1$ eV, the gas temperature $T = 300$ K and the electron density $n_e = 1.0 \times 10^{18} \text{ m}^{-3}$.

The atomic excited states above certain threshold energy are neglected in the model. In this way, an infinite number of species is reduced to a reasonable finite set. For the discussion and the methods for these neglected levels, we refer to a study by van Dijk *et al.* [17]. The Ar system contains totally 39 species including the ground, the excited states and the ion. The excited levels are chosen from smallest energy Ar(4s) group up to the energy level Ar(8j). Transition rates between these species are taken from [18]. Together with the ground state and the ion, Hg plasma contains 20 species. The excited levels range from Hg(6p1) group with the lowest energy to the level Hg(10p). The corresponding transition rates are adapted from [1].

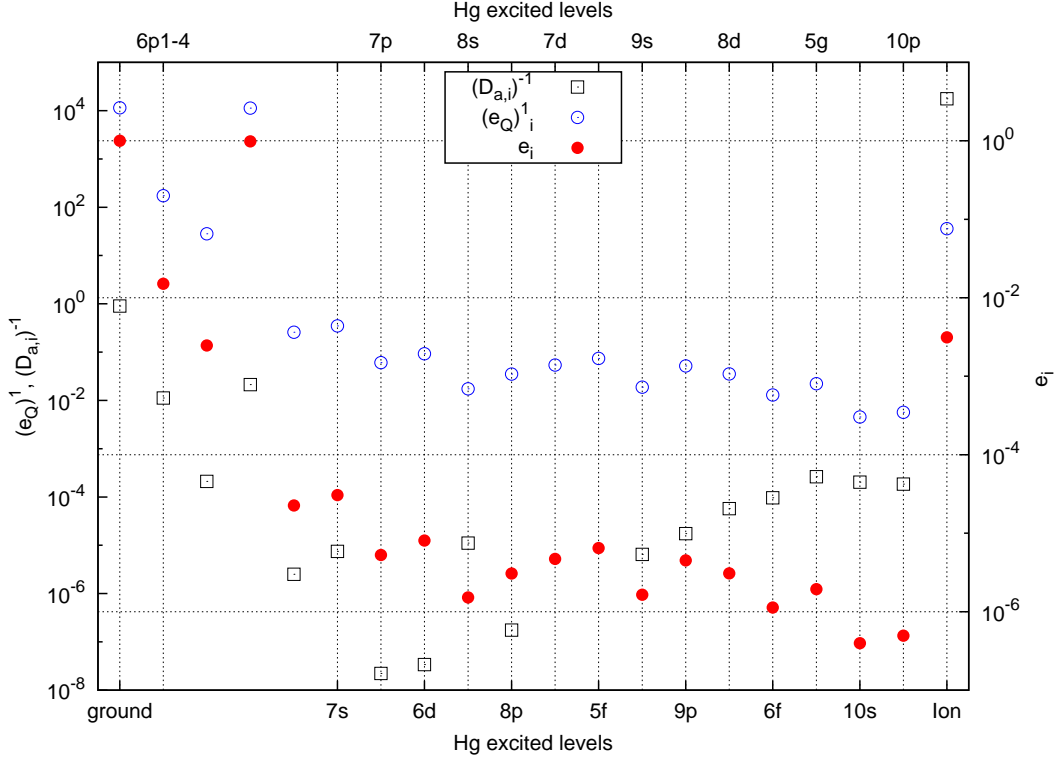


FIG. 5. (Mercury plasma) The density-independent consistent QSS error $(\mathbf{e}_Q)_i^1$, the inverse of Damköhler number $(D_{a,i})^{-1}$ and the error number e_i for numbered species (i). Note the double scales. Transport time-scale is $\tau_{tr} = 1.17 \times 10^{-03}$ s, which is determined via equation (53).

A. Transport frequency

The transport frequency is determined from the flux term in the particle balances. A fluorescent lamp has negligible convective flux and the diffusive transport satisfies [19]

$$\left| \vec{\nabla} \cdot D \vec{\nabla} n_i \right| = \frac{D}{\Lambda^2} n_i, \quad (53)$$

where Λ is the diffusion length and D is the diffusion coefficient. The coefficient D relates with the mean free path of elastic collisions λ and thermal velocity v_{th} : $D = 1/3 \lambda v_{th}$. The mean free path is $\lambda = \frac{1}{n\sigma}$, where n is the dominant gas density and σ is the momentum transfer cross-section. The thermal velocity satisfies $v_{th} = \sqrt{8k_B T_h / \pi m}$ where T_h is the gas temperature, m is the particle mass and k_B is the Boltzmann constant. We assume that the fundamental diffusion mode dominates [19]:

$$\frac{1}{\Lambda^2} = \frac{1}{\Lambda_0^2} = \left(\frac{\pi}{L} \right)^2 + \left(\frac{2.405}{R} \right)^2 \quad (54)$$

because the mean free path is smaller regarding the container dimensions. As a result, the transport frequency of neutrals is given by the relation

$$\nu_{tr} = \frac{\sqrt{8k_B T_h / \pi m}}{3n\sigma\Lambda_0^2}. \quad (55)$$

VII. RESULTS

We analyse the positive column of a fluorescent lamp for Ar and Hg respectively. In the analysis, we define that a parameter $r \ll 1$ if $r \leq \gamma$, where we set $\gamma = 1.0 \times 10^{-2}$. Within this definition, the density-independent QSS errors and the error numbers as well as the inverse of the Damköhler numbers are presented at the calculated transport frequencies. (The inverse values are shown for the sake of simplicity.) The classification of the species in CRM formalism is provided while the conventional and the novel conditions are compared. The maximum scale of the consistent QSS errors are presented for the LC levels and the consistent QSS errors are also shown for equilibrium density values.

The density-independent consistent QSS errors $(\mathbf{e}_Q)_i^1$, the error numbers e_i and the inverse of Damköhler numbers $(D_{a,i})^{-1}$ for Ar plasma are presented in Figure 4. The transport time-scale is calculated as $\tau_{tr} = 5.20 \times 10^{-04}$ s, using equation (53). In the system, the Ar(4s) group satisfies the QSS requirements according to the conventional condition. However, they have larger error numbers $e_i > 1.0 \times 10^{-2}$, hence, the novel condition suggests that they are TS instead. The rest of the species are classified LC, in agreement with the conventional method. Though Ar(7i) is defined as an LC level, it does not satisfy necessary conditions in both methods.

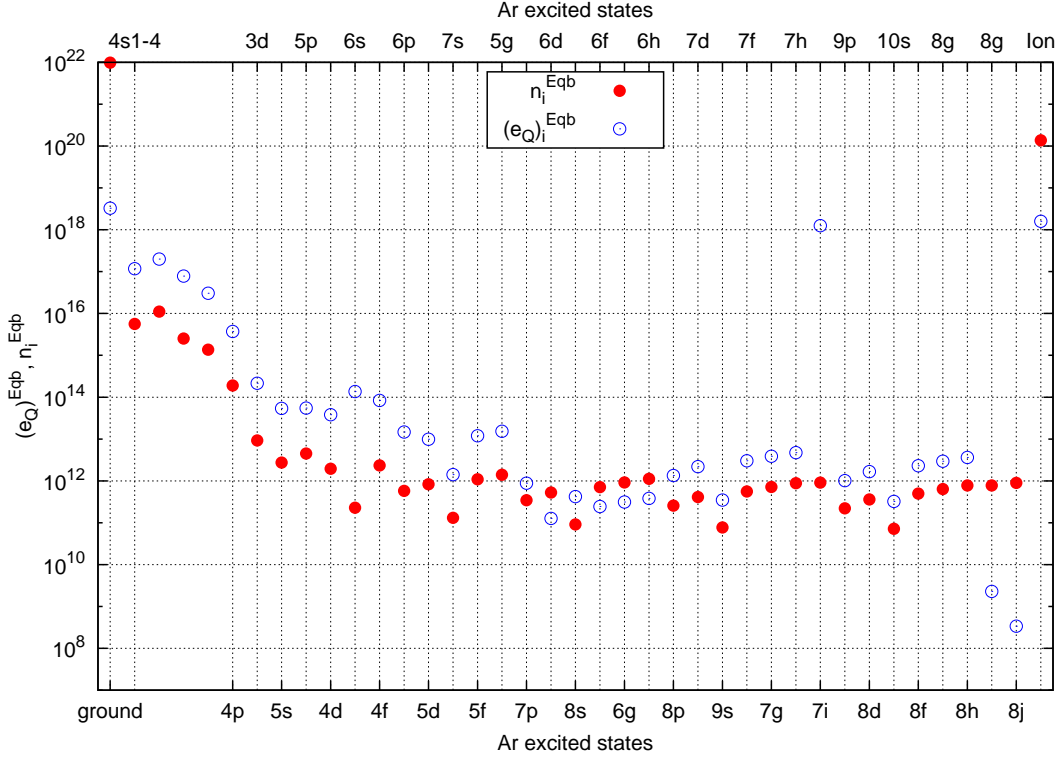


FIG. 6. The consistent QSS error $(e_Q)_i^{Eqb}$ for equilibrium density n_i^{Eqb} of the argon plasma. The transport time-scale is $\tau_{tr} = 5.20 \times 10^{-04}$ s.

We suspect that it is caused by a poor formulation of the regarding transitions. Within LC species, $(e_Q)_i^1$ determines a maximum value of QSS error $1.0 \times 10^{18} \text{m}^{-3} \text{s}^{-1}$ for $\text{Ar}(8g)$, $\text{Ar}(8j)$ and between $1.0 \times 10^{20} \text{m}^{-3} \text{s}^{-1}$ and $1.0 \times 10^{24} \text{m}^{-3} \text{s}^{-1}$ for the others.

Same quantities for Hg plasma are plotted at transport time-scale $\tau_{tr} = 1.0 \times 10^{-03}$ s in Figure 5. In this case, both conditions are in agreement. All excited levels qualify to be LC, while $\text{Hg}(6p1)$, $\text{Hg}(6p3)$ are TS levels. Upper bound of the density-dependent error ranges between $1.0 \times 10^{20} \text{m}^{-3} \text{s}^{-1}$ and $1.0 \times 10^{23} \text{m}^{-3} \text{s}^{-1}$, where large values belong to those excited levels neighbouring ground state.

In both systems, errors and error numbers decrease with the energy of the level in average while its slope lessens with energy. $D_{a,i}$ also follows a similar trend, while it shows colossal jumps at various levels compared to those of errors. We think that this behaviour is an effect of the local production comparable to the destruction at the specified times-scale. Both ground states have the highest error and numbers. The ions, on the other hand, are not classified by the number but assumed to be TS due to its complex transport properties.

We also present the consistent QSS errors $(e_Q)_i^{Eqb}$ at the equilibrium density distributions n_i^{Eqb} in Figures 6 and 7. The density distribution reduces the error compared to maximum values given by $(e_Q)_i^1$. The decrement is with a factor of 1.0×10^{-6} for argon while it is about

1.0×10^{-10} for mercury. On the other hand, their values relative to each other does not change.

VIII. SUMMARY AND CONCLUSION

We analyse atomic EEK plasmas and focus on the LC levels of the CRMs. These levels are assumed to be in QSS at a transport time-scale due to their large Damköhler number $D_{a,i} \gg 1$. This assumption is only valid in the case of a time-independent local production. However, the production implicitly depends on time via the densities. Furthermore, in CRMs, any kind of deviation from exact QSS behaviour and its role on the rest of the system is not quantified. In order to tackle this problem and describe the deviation, we analyse the plasma particle balance equations of all species in the diagonal basis of their source Jacobian. This analysis provides an approximate density-dependent source at the transport time-scale and we set its absolute value as the error of QSS assumption on the LC levels. In case the densities are not foreknown, we further define a density-independent error, which forms an upper bound of the error. Additionally, a dimensionless number is provided and sufficiently small number minimises the error and identifies a novel LC condition.

The technique is applied to the positive column of a fluorescent lamp with Ar and Hg separately. For the de-

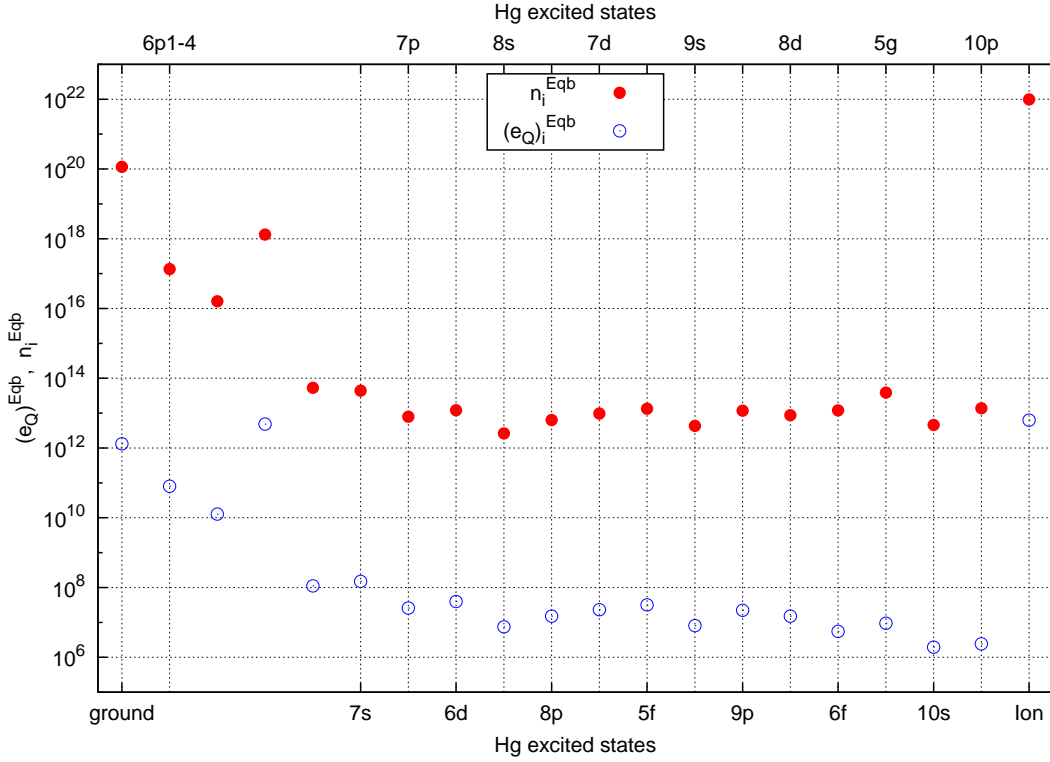


FIG. 7. The consistent QSS error $(\mathbf{e_Q})_i^{Eqb}$ for equilibrium densities n_i^{Eqb} of the mercury plasma. The transport time-scale is $\tau_{tr} = 1.17 \times 10^{-03}$ s.

finest transport time-scale, Ar(4s) group is identified to be a TS level, in contrast with the conventional condition. The rest possesses low error number $e_i < 0.01$, which classify them as LC levels. Ar(7i) substantially deviates from this. Though solid evidence lacks, it is reasonable that poor transition rate causes this deviation. The density-dependent error maxima ranges between $7.0 \times 10^{18} \text{ m}^{-3}\text{s}^{-1}$ and $1.0 \times 10^{24} \text{ m}^{-3}\text{s}^{-1}$. For Hg system, all excited states are LC species, except Hg(6p1), Hg(6p3) levels. The error maxima, in this case, ranges from $1.0 \times 10^{20} \text{ m}^{-3}\text{s}^{-1}$ to $1.0 \times 10^{23} \text{ m}^{-3}\text{s}^{-1}$.

In both systems, the density-independent error and the number decline with the energy of the excited level. This is in agreement with the fact that the energetic levels quickly settle in QSS compared to those with less energy. Additionally, the conventional QSS condition works for most of the levels but it can be inefficient for the low energy levels. For more accurate classification, the novel condition should be preferred.

The consistent QSS errors $(\mathbf{e_Q})_i^{Eqb}$ are also shown for equilibrium density distribution n_i^{Eqb} . Compared to the upper bound $(\mathbf{e_Q})_i^1$, their scale is significantly smaller. In this respect, the density-dependent errors should be used whenever the densities are available. On the other hand, the distribution $n_i(\tau_{tr}) = n_i^{Eqb}$ should be used with care, since it is only valid in the complete equilibrium.

We defined a γ parameter to describe a number that is negligibly small compared to unity. In this work, we set

it to $\gamma = 1.0 \times 10^{-2}$, yet its value is arbitrary. If smaller γ is chosen, then the description of a negligibly small value is further ensured. Additionally, it can set all species TS with a cost of higher computational burden in the CRM. Higher γ values can classify more excited species into LC levels, but they may still have large density-independent errors. In this case, the novel condition can exactly proceed parallel to the conventional technique. If it is too high (above 0.1) even the fast pseudo-species may not be negligible. At this point, the choice is left to the user. Depending on their needs, γ can be kept higher, while the resultant effect is defined by the QSS error. We suggest that this value should not exceed 0.1 since the source approximation is compromised by larger fast pseudo-densities.

The error is not determined continuously but rather discretely with the transport time-scale. The distribution of the eigenvalues determines these discrete points that should be also taken into account to compute the errors. In the analysed systems, the classification of the pseudo-densities and the errors are valid between $1.0 \times 10^{-5} \text{ s} < \tau_{tr} < 5.0 \times 10^{-3} \text{ s}$ for Ar and $1.0 \times 10^{-3} \text{ s} < \tau_{tr} < 5.0 \times 10^{-2} \text{ s}$ for Hg. As a caveat, around these discrete points the classification may change due to the arbitrary γ parameter. Furthermore, in this study the role of the initial density configuration is not taken into account in the classification. Excessively low initial pseudo-densities may qualify to be fast even before the criteria is met. Hence, the error and the error number can be

misleading around the discrete points of the eigenvalue distribution.

In the density-independent definitions, we choose the smallest 1-norm among the p-norms. This ensures that the maxima are kept closer to the density-dependent values compared to higher norms. Furthermore, the non-dimensionalisation constant ζ , which defines the error number e_i and the novel LC condition, imposes a QSS definition that is relative to ζ . In this study, ζ is chosen to be the maximum dimensionless QSS error. We ob-

serve that a different ζ parameter, such as the transport frequency of the plasma, increases the error number and changes the classification of the low energy states Ar(4p) and Hg(6p2).

The system is studied for reactions, where two distinct types of species interact. Otherwise, a source term that is a nonlinear function of the density vector appears. In the presence of these reactions, the method can be treated with source term linearisation within iterative schemes [2, 20].

-
- [1] J. van Dijk. *Modelling of Plasma Light Sources — an object-oriented approach*. PhD thesis, Eindhoven University of Technology, The Netherlands, 2001.
 - [2] R. L. G. M. Eggels. *Modelling of Combustion Processes and NO formation with Reduced Reaction Mechanism*. PhD thesis, Eindhoven University of Technology, The Netherlands, 1995.
 - [3] U. Maas and S. B. Pope. Simplifying chemical kinetics: Intrinsic low-dimensional manifolds in composition space. *Combustion and Flame*, 88:239–264, 1992.
 - [4] M. A. Lieberman and A. J. Lichtenberg. *Principles of Plasma Discharges and Materials Processing*. New Jersey: John Wiley Sons, 2005.
 - [5] D. Küppers and H. Lydtin. Preparation of optical waveguides with the aid of plasma-activated chemical vapour deposition at low pressures. *Topics in Current Chemistry*, 89:107, 1980.
 - [6] P. G. Flesch. *Light and light sources - High intensity discharge lamps*. Springer-Verlag, Berlin, 2006.
 - [7] D. R. Bates, A. E. Kingston, and R. W. P. McWhirter. Recombination between electrons and atomic ions, I. Optically thin plasmas. *Proc. R. Soc.*, A267:297, 1962.
 - [8] J. A. M. van der Mullen. Excitation equilibria in plasmas; a classification. *Phys. Rep.*, 191:109, 1990.
 - [9] D. A. Benoy, J. A. M. van der Mullen, B. van der Sijde, and D. C. Schram. A novel collisional radiative model with a numerical bottom and an analytical top. *J. Quant. Spectrosc. Radiat. Transfer*, 46(3).
 - [10] J. van Dijk, B. Hartgers, J. Jonkers, and J. A. M. van der Mullen. Collisional radiative models with multiple transport-sensitive levels - application to high electron density mercury discharges. *J. Phys. D: Appl. Phys.*, 34(10).
 - [11] M. Stiefenhofer. Quasi-steady-state approximation for chemical reaction networks. *J. Math. Biol.*, 36:593–609, 1998.
 - [12] H. G. Kaper and T. J. Kaper. Asymptotic analysis of two reduction methods for systems of chemical reactions. *Physica D: Nonlinear Phenomena*, 165:66–93, 2002.
 - [13] N. Peters and B. Rogg. *Reduced Kinetics Mechanisms for Applications in Combustion Systems*. Springer verlag, 1993.
 - [14] R. T. Skodje and M. J. Davis. Geometrical simplification of complex kinetic systems. *J. Phys. Chem A*, 105:10356–10365, 2001.
 - [15] K. Beks-Peerenboom. *Modelling of Magnetized Expanding Plasmas*. PhD thesis, Eindhoven University of Technology, The Netherlands, 2012.
 - [16] G. R. Rogoff. Ambipolar diffusion coefficients for discharges in attaching gases. *J. Phys. D: Appl. Phys.*, 18.
 - [17] J. van Dijk, A. Hartgers, J. Jonkers, and J. A. M. van der Mullen. A collisional radiative model for mercury in high-current discharges. *J. Phys. D: Appl. Phys.*, 33:2798, 2000.
 - [18] D. A. Benoy. *Modelling of thermal argon plasmas*. PhD thesis, Eindhoven University of Technology, The Netherlands, 1993.
 - [19] P. J. Chantry. A simple formula for diffusion calculations involving wall reflection and low density. *J. Appl. Phys.*, 62:1141, 1987.
 - [20] S. V. Patankar. *Numerical Heat Transfer and Fluid Flow*. New York: McGraw-Hill, 1980.